ERDC/EL TR-20-7

US Army Corps
of Engineers®
Engineer Research and
Development Center

ERDC
ENGINEER RESEARCH & DEVELOPMENT CENTER

*Coastal Ocean Data Systems Program*

# Evaluation of Unmanned Aircraft System Coastal Data Collection and Horizontal Accuracy: A Case Study at Garden City Beach, South Carolina

Molly Reif, Scott Bourne, Jennifer Laird, Thomas Berry,
Justin Wilkens, Kevin Philley, and Kenneth Matheson

September 2020

Environmental Laboratory

**The US Army Engineer Research and Development Center (ERDC)** solves the nation's toughest engineering and environmental challenges. ERDC develops innovative solutions in civil and military engineering, geospatial sciences, water resources, and environmental sciences for the Army, the Department of Defense, civilian agencies, and our nation's public good. Find out more at www.erdc.usace.army.mil.

To search for other technical reports published by ERDC, visit the ERDC online library at https://erdclibrary.on.worldcat.org/discovery.

ERDC/EL TR-20-7
September 2020

# Evaluation of Unmanned Aircraft System Coastal Data Collection and Horizontal Accuracy: A Case Study at Garden City Beach, South Carolina

Molly Reif

*Environmental Laboratory*
*US Army Engineer Research and Development Center*
*Joint Airborne Lidar Bathymetry Technical Center of Expertise*
*7225 Stennis Airport Rd, Suite 100*
*Kiln, MS 39556*

Scott Bourne, Jennifer Laird, Thomas Berry, Justin Wilkens, Kevin Philley, and Kenneth Matheson

*Environmental Laboratory*
*US Army Engineer Research and Development Center*
*3909 Halls Ferry Road*
*Vicksburg, MS 39180*

Final report



Prepared for Coastal Ocean Data Systems Program
USACE Engineer Research and Development Center
Coastal and Hydraulics Laboratory
Vicksburg, MS 39180-6199

Under AMSCO 190012, “UAS Support for Coastal Management”

# Abstract

The US Army Corps of Engineers (USACE) aims to evaluate unmanned aircraft system (UAS) technology to support flood risk management applications, examining data collection and processing methods and exploring potential for coastal capabilities. Foundational evaluation of the technology is critical for understanding data application and determining best practices for data collection and processing. This study demonstrated UAS Multispectral (MS) and Red Green Blue (RGB) image efficacy for coastal monitoring using Garden City Beach, South Carolina, as a case study. Relative impacts to horizontal accuracy were evaluated under varying field scenarios (flying altitude, viewing angle, and use of onboard Real-Time Kinematic–Global Positioning System), level of commercial off-the-shelf software processing precision (default optimal versus high or low levels) and processing time, and number of ground control points applied during postprocessing (default number versus additional points). Many data sets met the minimum horizontal accuracy requirements designated by USACE Engineering Manual 2015. Data collection and processing methods highlight procedures resulting in high resolution UAS MS and RGB imagery that meets a variety of USACE project monitoring needs for site plans, beach renourishment and hurricane protection projects, project conditions, planning and feasibility studies, floodplain mapping, water quality analysis, flood control studies, emergency management, and ecosystem restoration.

# Contents

# Figures and Tables

## Figures



## Tables

# Preface

This report was funded by the US Army Corps of Engineers (USACE) Coastal and Ocean Data Systems (CODS) program under the "Unmanned Aircraft Systems Support to Coastal Management" work unit. Data collection informing the report was funded by the Office of Homeland Security, USACE. The CODS work unit has also been leveraged with research within the "UAS Support to Flood Risk Management" work unit, funded by the Flood and Coastal Systems (F&CS) R&D Program.

The CODS and F&CS programs are administered at the USACE Engineer Research and Development Center Coastal and Hydraulics Laboratory (ERDC-CHL). At the time this effort was conducted, Dr. Jeffrey P. Waters, Coastal Observations and Analysis Branch was Program Manager of CODS. Mr. Charles E. Wiggins was the Technical Director for Navigation. Mr. Michael E. Ott was the Navigation Business Line Manager. Dr. Brandon M. Boyd was the Program Manager of F&CS R&D and Associate Technical Director of Flood and Coastal Systems Risk Management R&D. Dr. Julie D. Rosati was the Lead Civil Works Technical Director for R&D as well as the Technical Director for Flood and Coastal Risk Management R&D. Mr. Mark S. Roupas, HQUSACE, was Deputy Chief, Office of Homeland Security, USACE, as well as FRM Business Line Manager.

The work was performed by the Environmental Systems Branch of the Ecosystem Evaluation and Engineering Division, ERDC Environmental Laboratory (ERDC-EL). Technical reviews and discussions of this report were provided by Jeffrey G. Ruby of the ERDC Geospatial Research Laboratory and Nicholas J. Spore of ERDC-CHL. At the time of publication of this report, Mr. Mark Graves was Branch Chief; Mr. Mark Farr was Division Chief; Dr. Jeffrey P. Waters was Branch Chief; and Dr. Cary A. Talbot was Division Chief. The Director of ERDC-CHL was Dr. Ty V. Wamsley.

COL Teresa Schlosser was the Commander of ERDC, and the Director was Dr. David W. Pittman.

# 1 Introduction

## 1.1 Background

Remote sensing technology is being increasingly used to monitor continuously evolving, complex coastal ecosystems. More specifically, airborne and spaceborne platforms are used to characterize or identify critical coastal habitats, such as wetlands, submerged aquatic vegetation, and coral reefs at varying levels of detail and accuracy (Klemas 2001; Klemas 2013; Mumby et al. 1995; Phinn et al. 2000). Qualitative and quantitative data describing habitat conditions and trends can be useful for monitoring coastal changes that impact important ecosystem services, such as erosion and water flow regulation. Additionally, coastal restoration activities are likewise increasing, as the role for coastal systems and associated habitats to protect inland areas through increasing stability and reducing erosion from storm-related wind and wave energy are better understood and quantified.

Recently, USACE has identified a need to evaluate unmanned aircraft system (UAS) technology to support flood risk management applications, examining data collection and processing methods and exploring potential for coastal capabilities, including ecosystem characteristics, which are a critical component to resiliency and recovery (Bruder et al. 2018; Suir et al. 2018). As part of this research need, an initial field experiment was held at the USACE Field Research Facility in Duck, North Carolina, in which multiple agencies, academia, and private industry conducted a coordinated UAS and field data collection campaign in June 2017 (Bruder et al. 2018). During this experiment, a variety of sensors and platforms were operated with coordinated ground and air missions to better compare imagery and derived data products to inform flood risk management tools and models. Subsequent to that experiment and as part of ongoing research, USACE identified various pilot studies at district offices to evolve and enhance UAS practices within specific application contexts during the summer and fall of 2018. This opportunity allowed for meetings with districts currently implementing coastal projects that could benefit from a UAS survey, ranging from dredging operations to shore protection, while simultaneously affording ERDC the ability to evaluate UAS operations. As a result, the EL team worked with the USACE Charleston District (SAC) to identify and discuss suitable project topics for

evaluation and implementation of UAS technology, building upon lessons learned from the field experiment at Duck, North Carolina. Coastal restoration, including renourishment in 2017 and planting and fencing in 2018, occurred along two reaches of the Myrtle Beach Shore Protection Project and would serve as a suitable opportunity to evaluate the collection of imagery and ground data that could be used to support coastal monitoring efforts.

As reviewed by Suir et al. (2018), UAS technology to support USACE environmental applications related to flood risk management have shown promise for poststorm ecosystem damage assessment, geomorphic effects from major flooding events, levee monitoring and impacts, and avian and wildlife habitat surveys. Moreover, the technology has potential to complement traditional field-based surveys (Acosta et al. 2005), in which impacts to sensitive, restored environments can be minimized, and to existing airborne and spaceborne surveys (Wozencraft et al. 2018), helping to fill in data gaps, including temporal and spatial coverage as well as spatial detail. Specific to coastal applications, UAS technology has been tested to assess the following:

- beach topography and morphology, such as through Structure from Motion (SfM) (Chen et al. 2018; Goncalves and Henriques 2015; Mancini et al. 2013; Seymour et al. 2018)
- coastal surveying and beach erosion (Scarelli et al. 2017; Turner et al. 2016)
- sand burial to better understand dune grass growth response (Nolet et al. 2018)
- estimating fractional vegetation cover (Choi et al. 2016)
- coastal structure assessment for coastal engineering (Drummond et al. 2015)
- dune growth dynamics (van Puijenbroek et al. 2017)
- geomorphic feature extraction and land cover classification (Sturdivant et al. 2017)
- beach zone identification using Red Green Blue (RGB) imagery (Su and Gibeaut 2017)
- other diverse environmental monitoring and mapping applications(Green et al. 2019; Klemas 2015)

As UAS applications continue to be explored, foundational evaluation of the technology is critical for understanding data application and

determining best practices for data collection and processing. Given the high level of spatial, spectral, and structural detail of UAS data, it could be useful to complement the existing suite of coastal monitoring tools. However, it is first beneficial to assess UAS data accuracy for such an application, especially in relation to data collection and processing methods. This is particularly true for assertions that time-consuming collection of ground control points (GCPs) is not necessary because of UAS incorporation of internal Real-Time Kinematic–Global Positioning System (RTK-GPS) for high positional accuracy (Turner et al. 2016).

## 1.2 Objective(s)

The goal of this study was to demonstrate UAS Multispectral (MS) and Red Green Blue (RGB) image efficacy collecting and processing images with horizontal accuracy sufficient for coastal applications, such as dune vegetation restoration monitoring near Garden City Beach, South Carolina (GCB). More specifically, the objectives were to evaluate the relative impacts to horizontal accuracy under differing data collection scenarios, number of GCPs applied during postprocessing, and level of precision applied using commercial off-the-shelf software (including variances in processing time).

## 1.3 Approach

The approach of this study is presented in chapter 2.

# 2 Data and Methods

## 2.1 Site description

The study area was located at GCB, bordering the Atlantic Ocean and south of the city of Myrtle Beach. The GCB 7.8 km[1] coastline begins in the southern end of Horry County and extends south into Georgetown County, ending at Murrells Inlet. The GCB is primarily a residential development with significant growth post-1950s consisting of beach houses, condominiums, and summer rentals. The surveyed area was a 600 m linear section of GCB coastline, located within the southern end of Reach 3, a 12.4 km segment in the SAC Myrtle Beach Shore Protection Project, which is a storm damage reduction project (figure 1). In October 2016, Hurricane Matthew made landfall about 64 km south of the study area resulting in substantial beach erosion. In 2017, beach renourishment and dune construction occurred, and in March and April, 2018, *Panicum amarum* Elliott 'Northpa' (bitter panicum) and *Uniola paniculata* L. (sea oats) were planted on the dunes. Over 9,000 m of fencing was installed in Reach 3 between the shoreline and the perpetual easement line. More specifically, two rows of fencing were installed in a V-shaped pattern with gaps allowed for wildlife movement, while in the vicinity of GCB, a total of 14 vegetation rows were planted across the renourished area. Starting on the ocean side of the fencing, the first 6 rows are bitter panicum and the next 8 rows, moving landward, are sea oats. Rows were spaced approximately 0.46 m apart, and plant spacing is 0.61 m. The area surveyed includes the fencing and dune vegetation (stations 100–120 and public access points 10–22) as reported in the Myrtle Beach Reaches 1 & 3 Sand Fencing and Dune Vegetation Shore Projection Project Plans and Specifications (USACE 2017).

1. For a full list of the spelled-out forms of the units of measure used in this document, please refer to *US Government Publishing Office Style Manual*, 31st ed. (Washington, DC: US Government Publishing Office, 2016), 248–52, https://www.govinfo.gov/content/pkg/GPO-STYLEMANUAL-2016/pdf/GPO-STYLEMANUAL-2016.pdf.

Figure 1. Garden City Beach, South Carolina (GCB), study area.


## 2.2 Data collection

The ERDC-EL conducted UAS flights during August 7–9, 2018, at GCB. This location is under the Class G airspace, and all UAS operations were properly conducted and coordinated with both the Federal Aviation Administration (FAA) and the USACE Aviation program. In accordance with the FAA Part 107 Remote Pilot Certification, all pilots and visual observers maintained visual line of sight (VLOS) with the UAS at all times. Flights were planned to maintain VLOS for all flights and were flown in appropriate weather conditions for ideal operations of the sensor and platform. Since the survey area included a public beach, daily operations were assisted by and coordinated with the Georgetown County Department of Public Services. Public access points were used to transport equipment using a Polaris All Terrain Vehicle and mark the survey area boundary with orange cones, caution tape, and signs (figure 2), which were placed every morning prior to operations and removed each day after operations were completed. This process helped to communicate the

purpose of the survey to the public while reducing human traffic inside the survey area. Furthermore, care was taken not to block or impede beach access, since August is a busy time in the tourist season, and boundary markers were placed landward of the high-tide line by at least 3 m. In general, each survey day included setup of a UAS and GCP deployment and operations base just outside the survey area (for UAS takeoffs and landings) and was located at either the north or south end of the survey area. Total time for equipment transit, boundary marking, UAS setup and deployment, flight operations, and breakdown ranged between 8 to 10 hours each day.

Figure 2. Sign used to help demark the survey area and communicate survey plans to the public.


A hybrid fixed-wing UAS (FireFly6 Pro, BirdsEyeView Aerobotics, Andover, New Hampshire, USA) equipped with a 5-band MS (RedEdge-M, MicaSense, Seattle, Washington) or an RGB digital camera (Sony a7R 36MP, Sony Corporation, Tokyo, Japan) was used to collect images using default camera settings (figure 3). Table 1 lists the MS band names, centers, and widths, while table 2 lists the camera settings. The UAS platform is a hybrid system because it has the ability to vertically ascend to altitude, where it transitions into forward flight for the duration of the mission. A survey mission was created using the BirdsEyeView FireFly6 Planner version 2.3 software on a Panasonic Toughbook CF-30. During a mission, vertical takeoff and transition to forward flight was manually controlled by the UAS pilot. Once the UAS was confirmed to be operating

normally in manual mode, the survey was started, and the remainder of the mission was completed autonomously. Upon completion of the survey, the UAS was transitioned to vertical flight and manually landed by the pilot, thus completing the mission.

Table 1. List of MS camera band names, centers, and widths (units are in nanometers [nm]).

| MS Band | Center wavelength | Bandwidth |
|---|---|---|
| Blue | 475 | 32 |
| Green | 560 | 27 |
| Red | 668 | 16 |
| RedEdge | 717 | 12 |
| Near Infrared | 840 | 57 |

Table 2. List of MS and RGB camera settings.

| Camera | Flying altitude (m) | Focal length (mm) | Pixel array | Field of view horizontal (m) | Field of view vertical (m) |
|---|---|---|---|---|---|
| RGB | 60 | 28 | 7360 × | 76.9 | 51.4 |
| RGB | 120 | 28 | 7360 × | 153.9 | 102.9 |
| MS | 60 | 5.5 | 1280 × | 52.4 | 39.3 |

In total, 20 flights were flown with the UAS system, including two test flights. Data collection with the MS sensor consisted of a total of 15 missions, while 5 missions were completed with the RGB sensor. A total of nine data sets, including five MS and four RGB, were selected for processing and image analysis to ensure a variety of sensor and data collection scenarios (for example, different altitudes and viewing angles). Flight times varied depending on the sensor deployed and ranged from 4 to 18 minutes, with an average of 10 minutes for each mission. Local solar noon time at GCB was 13:30, and all data collections were flown ±2 hours from solar noon for the best image quality, minimizing shadows and improving reflectance measurements. Skies were generally clear, and wind conditions stayed fairly consistent at 5–7 mph, with one day at 12 mph that caused image quality issues, and thus, those data were not selected for processing.

Figure 3. BirdsEyeView FireFly6 Pro UAS used to survey the study area at GCB.

For improved accuracy of the Global Positioning System (GPS), the UAS system has an onboard RTK-GPS that improves both the vertical and horizontal accuracies of the system and resultant data products. While the majority of the flights were conducted using the RTK-GPS, one flight with the MS sensor was flown without it on August 7 to evaluate the impacts to horizontal accuracy on the imagery. While RTK is used to improve data accuracy without the reliance on GCPs, there are still limitations with full time RTK due to the potential loss of GPS signal during any aerial survey. In fact, there were some signal disruptions experienced during several of the flight collections. All MS flights were flown in a racetrack pattern, with 60% side overlap and 60% frontal overlap at 60 m height above ground level (AGL) parallel to the shoreline with the sensor in a NADIR (looking directly down under the UAS) position. The RGB camera was flown at both 120 and 60 m AGL with either 60% side overlap and 80% frontal overlap or 80% overlap for both the frontal and side. In addition, the RGB camera was flown at NADIR and 10°off-NADIR (two flights with sensor pointed at 10°) position to evaluate the effect of the viewing angle on horizontal accuracy.

## 2.3 Ground control and field data

A base station receiver was established near the UAS launch area, from which the UAS received location error correction inputs during missions. Near the UAS launch area, one GPS unit (Trimble R10) was placed in a stationary location (base), in this case a temporary stake, for over two

hours, collecting raw data at a rate of 1-30 Hz. At the end of each day, the base location raw data were uploaded to the National Oceanic and Atmospheric Administration (NOAA) National Geodetic Survey (NGS) Online Positioning User Service (OPUS), where the raw data were compared to several permanent reference GPS stations. This method provided coordinates for the control mark in the International Global Navigation Satellite System (GNSS) Service (IGS) 2008 (IGS08), World Geodetic System 1984 Reference (WGS84) Coordinate System, and elevation coordinates with an Ellipsoid elevation and ground surface orthographic heights (North American Vertical Datum 1988) using Geoid model 12B.

Ground control was accomplished by placing a survey-grade, dual frequency Trimble R10 GPS unit on a temporary monument located next to a fence post on the south end of the survey area. GPS signals collected and retransmitted from this location served to establish another temporary georeferenced position for the GPS used on the aircraft and to RTK-GPS surveys of preconstructed GCPs placed within the survey area, including points in the dunes and along the beach. Rapid positions are usually available from OPUS within three hours of data collection, and they are typically within 5 cm ($x$, $y$, and $z$) of the precise position. This method establishes precise positions, which are used during UAS missions to provide corrections to the imagery and to send corrections to roving GPS units conducting the ground truth surveys. Precise OPUS positions are available approximately three weeks after the data is collected, and, depending upon accuracy requirements of the data, the location of the base GPS receiver can be updated at that time, resulting in more precise ground control coordinates.

Initially, the GCP surveys were conducted using two Trimble R10 GPS units operating in the RTK mode. This method established coordinates ($x$, $y$, and $z$) on the visual markers, or GCPs, to within 5 mm horizontal and 1 cm vertical, referenced back to the base location. The RTK positions were collected on the GCPs visible in both the RGB and MS images collected by the UAS. There were 32 GCPs placed and surveyed for each flight. A GCP consisted of a five-gallon bucket lid (≈30 cm diameter) spray-painted black with a CD (12 cm diameter) glued in the middle, reflective side up (figure 4). This GCP was created to contrast with the light color background of the sand.

Figure 4. Example of a Ground Control Point (GCP) target used to process the UAS imagery.

Despite onboard RTK-GPS, GCPs are recommended for corridor mapping projects, in which the survey area dimensions are significantly larger in one dimension than other (https://support.pix4d.com/hc/en-us/articles/202559299-Number-and-distribution-of-ground-control-points-GCPs-in-corridor-mapping). This applies to coastal projects, which are often long and rectangular. In such cases, offset arrangement of GCPs is typically recommended. In this study, GCPs were placed in three rows spaced 15 m apart in the 600 × 60 m study area, with lids approximately 60 m apart along the rows. On the two outside rows (one in the dunes and one on the open beach), the lids were placed evenly across from each other, each row having 11 lids. This number and distribution provided an abundance of GCPs to use for postprocessing as well as for checkpoints in the independent evaluation of the horizontal accuracy; however, it is important to note that this many GCPs are not required in this type survey. Due to the tide level, the row of bucket lids on the beach had to be adjusted each day, and thus, there was slightly different ground truth each day. Altogether, there were three offset rows of GCPs for the flights, 32 points each (figure 5).

Figure 5. GCP distribution at GCB.

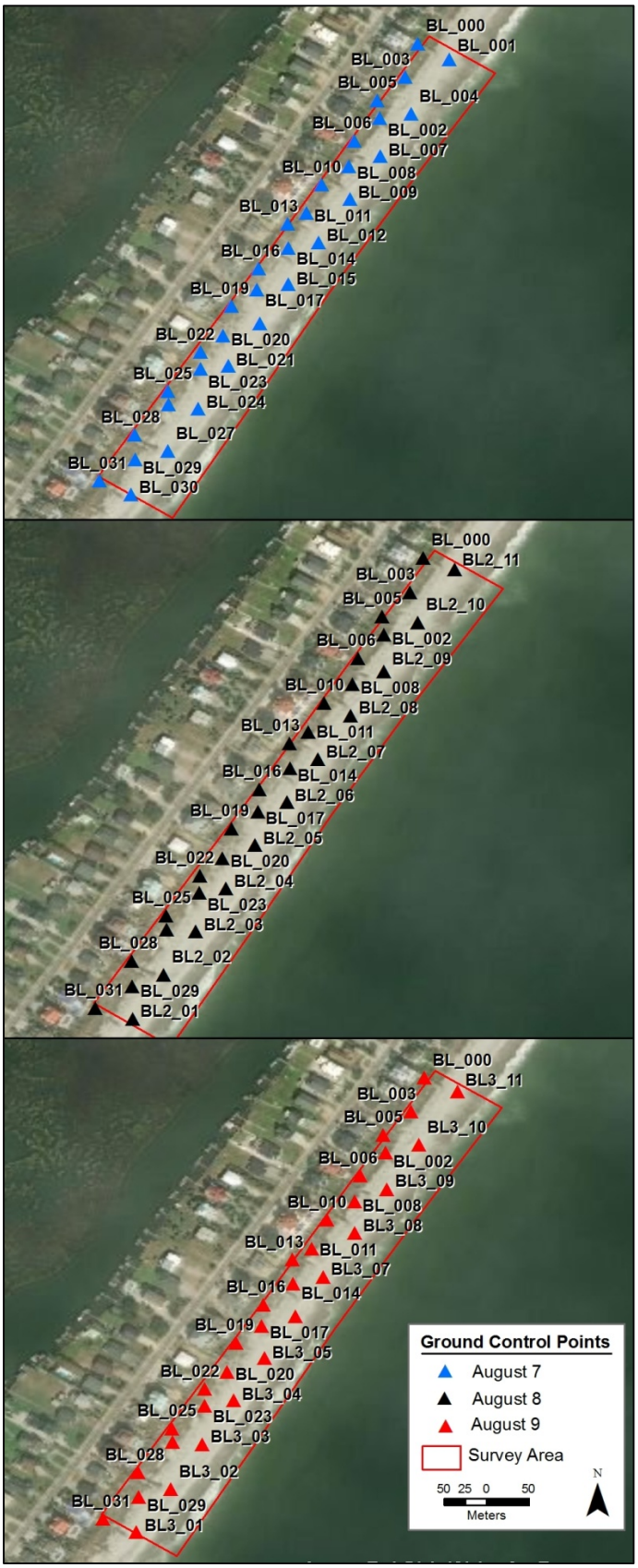

In addition to GCPs, additional field data were collected to support future dune vegetation analyses, including field measurements collected by a plant identification expert. For this application, horizontal accuracy is particularly important in order to best compare image-derived values with field measurements for characterization of vegetation that may be useful for monitoring. In this study, a modified point intercept method was designed with a structured *W* layout (figure 6), consisting of multiple connected transects oriented perpendicular to the shore and covering three zones: the outer sparse foredune, central dune area with targeted plant species (that is, focus area), and landward side of the dune with possible remnant vegetation (Thomas et al. 2007). This method was implemented in five locations to reduce sampling time while maximizing coverage within the study area. Transects with multiple segments have the potential to induce sampling bias for probabilities of selection near boundaries (Affleck et al. 2005), but they have limited implications as applied here, because points will be used to train remotely sensed data corresponding to ground truthed elements. Also, the study area was planted with two grass species in predetermined zones with limited recruitment by volunteer species. The transect lengths extended beyond these zones into the unvegetated portion of the upper beach and portions of the dunes outside the primary area of interest. Points established at 1 m intervals were expanded to 4 $cm^2$ positioned diagonally underneath the transect tape. Elements occurring within the 4 $cm^2$ including vegetation, sand, soil, and debris were recorded in descending order of estimated percent cover. Notes on health and vigor of plant species were recorded to account for potential anomalies in reflectance values that might be induced by inflorescences, fruits, and chlorotic or necrotic tissues. The 1 m spacing prevented individual plants from being selected by more than one point, with the exception of species with prostrate or vine-like growth forms. Measurements included the following:

- High accuracy latitude and longitude with survey grade GPS
- Plant species, estimated height, and health characteristics
- Spectral reflectance of the dominant plant species using a handheld Analytical Spectral Devices spectroradiometer (visible to near infrared) at select sites
- GPS tagged photographs.

Figure 6. Modified point intercept method with a structured *W* layout used to conduct dune vegetation sampling.


## 2.4 Data processing workflow and parameters

Nine MS and RGB data sets were processed using Pix4DMapper software (version 4.3.3.31) to generate reflectance and orthomosaic image products and evaluate impacts to horizontal accuracy from the following:

1. Various field scenarios (flying altitude, viewing angle, onboard RTK-GPS)
2. Level of software processing precision (default optimal level vs. high or low levels) and processing time
3. Number of GCPs applied during postprocessing (default number vs. additional points)

Coordinate system information for the images was WGS84 (EGM96 Geoid) and the output coordinate system was WGS84/UTM Zone 17N (EGM96 Geoid).

Internal camera calibration for the RGB sensor was already accounted for in the Pix4DMapper software that is gathered when imagery is loaded into the system. For the MS sensor, the calibration parameters specific to the sensor were obtained from the manufacturer. Before each flight, MS imagery was captured over a calibration panel specific to the sensor and provided by the manufacturer (figure 7), while a down-welling light sensor (DLS) mounted on the UAS platform helped account for lighting conditions and overall radiometric quality. The panel helps ensure calibration and confirms information collected by the DLS. As such, table 3 lists the manufacturer-provided reflectance values entered into Pix4DMapper software to correct the light balance in the images. Selection in Pix4D for the radiometric correction type was set to Camera and Sun Irradiance. The MS processing resulted in five, individual orthomosaics (one per band) that were georectified and calibrated within Pix4Dmapper software. Then, ENVI version 5.4.1 software was used to combine the five orthomosaics into a single composite image prior to the horizontal accuracy assessment.

Figure 7. Reflectance calibration panel imaged before each MS mission.

Table 3. List of manufacturer-provided, sensor-specific reflectance values used for radiometric calibration of the MS imagery in the Pix4DMapper software.

| MS band | Absolute reflectance value |
|---|---|
| Blue | 0.493 |
| Green | 0.494 |
| Red | 0.495 |
| RedEdge | 0.495 |
| Near Infrared | 0.494 |

### 2.4.1 Default processing parameters

Pix4DMapper software has many options and parameter settings. For this study, a set of standard, or default, processing settings were selected to hold constant to facilitate data comparisons. The nine data sets collected under various field scenarios were processed with the default parameters described below (https://support.pix4d.com/hc/en-us/articles/202557799-Menu-Process-Processing-Options-2-Point-Cloud-and-Mesh-Point-Cloud). The key point image scale was set to full to allow for increased key point generation on the imagery due to the homogenous background of the sand on the beach.

- Minimum number of matches was set to 3: "Each 3D point has to be correctly re-projected in at least 3 images"
- Image scale was set to multiscale, 1/2 (half image size): "The *image scale* defines the scale of the images at which additional 3D points are computed. Half size images are used to compute additional 3D points and it is the recommended image scale"
- Optimal point density: "A 3D point is computed for every (4/ *Image Scale)* pixel. For example, if the *Image Scale* is set to *1/2 (half image size)*, one 3D point is computed every 4/(0.5) = 8 pixels of the original image. This is the recommended point cloud density."

In addition to the settings listed above, the Pix4DMapper software recommended six GCPs as the default or suitable number to use in postprocessing for image production. GCPs were manually selected keeping in mind the software-recommended offset arrangement of GCPs for corridor mapping.

### 2.4.2 Field scenario parameters

Many factors can affect the positional accuracy of the final orthomosaic. These factors include parameters and sensor setup used during the

collection of the imagery (for example, field scenarios). This analysis compares the differences in horizontal imagery due to varying the following:

1. Flying altitude (60 vs 120 m)
2. Viewing angle (NADIR vs 10° off-NADIR)
3. Onboard RTK-GPS (corrected vs not corrected; using a UAS base receiver transmitting National Spatial Reference Systems (NSRS) coordinates obtained using the OPUS)

Table 4 lists the nine data sets processed, including the field scenarios used during the acquisition of the images and the software's default processing options used. Figures 8 and 9 show examples of the reflectance image products. The spatial resolutions of the MS and RGB imagery examples are 0.036 m and 0.015 m, respectively.

Table 4. List of the evaluated UAS data sets at GCB.

| Date | Flight | UAS Base Receiver RTK Corrected | Number of Processing GCPs | Viewing Angle | Altitude (m) | Ground Sampling Distance (m) | Software Processing Precision Level | Sensor |
|---|---|---|---|---|---|---|---|---|
| 8/7/2018 | F2 | No | 6 | NADIR | 60 | 0.0353 | Optimal | MS |
| 8/8/2018 | F2 | Yes | 6 | NADIR | 60 | 0.0364 | Optimal | MS |
| 8/8/2018 | F3 | Yes | 6 | NADIR | 60 | 0.0363 | Optimal | MS |
| 8/8/2018 | F6 | Yes | 6 | NADIR | 60 | 0.0357 | Optimal | MS |
| 8/8/2018 | F7 | Yes | 6 | NADIR | 60 | 0.0363 | Optimal | MS |
| 8/9/2018 | F2 | Yes | 6 | 10° | 120 | 0.0148 | Optimal | RGB |
| 8/9/2018 | F3 | Yes | 6 | NADIR | 120 | 0.0145 | Optimal | RGB |
| 8/9/2018 | F4 | Yes | 6 | NADIR | 60 | 0.0069 | Optimal | RGB |
| 8/9/2018 | F6 | Yes | 6 | 10° | 60 | 0.0072 | Optimal | RGB |

Figure 8. MS image example (Flight F6) from August 8, 2018, with insets showing examples of dune vegetation restoration (fencing and planting matrix).

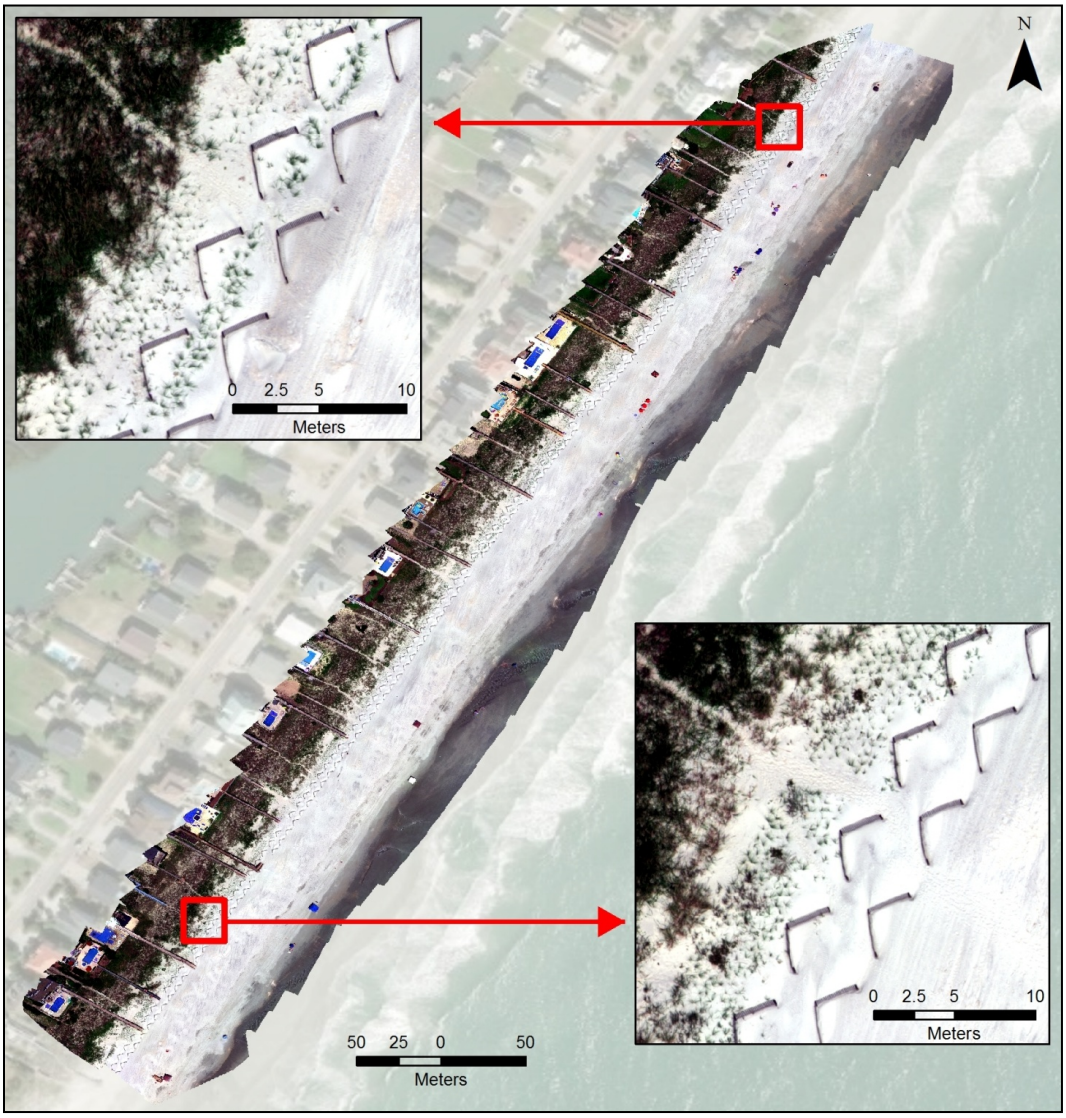

Figure 9. RGB image example (Flight F3) from August 9, 2018, with insets showing examples of dune vegetation restoration (fencing and planting matrix).


### 2.4.3 Software processing precision level parameters

Orthomosaic products were generated to evaluate horizontal accuracies in relation to differences in the Pix4DMapper software processing precision levels. More specifically, processing precision refers to point density, or the density of the point cloud in three levels: Optimal (default), High, and Low, described as follows (https://support.pix4d.com/hc/en-us/articles/202557799-Menu-Process-Processing-Options-2-Point-Cloud-and-Mesh-Point-Cloud):

- Optimal (Default): "A 3D point is computed for every (4/ *Image Scale)* pixel. For example, if the *Image Scale* is set to *1/2 (half image size)*,

one 3D point is computed every 4/(0.5) = 8 pixels of the original image. This is the recommended point cloud density."

- High (Slow): "A 3D point is computed for every *Image Scale* pixel. The result will be an oversampled Point cloud that requires up to 4 times more processing time and RAM than optimal density. Usually, this point cloud option does not significantly improve the results."
- Low (Fast): "A 3D point is computed for every (16/*Image Scale)* pixel. For example, if the *Image Scale* is set to *1/2 (half image size)*, one 3D point is computed every 16/(0.5) = 32 pixels of the original image. The final point cloud is computed up to 4 times faster and uses up to 4 times less RAM than optimal density."

#### *2.4.3.1 Software processing time methods*

Data processing hardware parameters are listed in table 5.

Table 5. Data processing hardware parameters.

| CPU | RAM | GPU | Operating System |
|---|---|---|---|
| Intel ® Xenon ® CPU E5-2697 v2 @2.70GHz | 128GB | NVIDIA Quadro K4000 | Windows |

Timing tests were performed to provide a simple cost-benefit analysis of the different settings in the software, with cost reflected as the amount of time to process an image. Pix4D processing times were observed at various processing precision levels (Optimal, High, and Low) for the generation of reflectance mosaics, orthomosaics, and point clouds for the same two flight examples, MS flight F2 (August 8) and RGB flight F4 (August 9). This was done to observe the potential influence of software processing times and precision levels on the horizontal accuracy.

### 2.4.4 Number of GCPs applied during postprocessing parameters

RTK-corrected imagery was processed using no GCPs and either 6 (default number recommended by the software), 8, or 10, GCPs. Increasing the default value incrementally by two allowed for the careful evaluation of potential accuracy differences while ensuring there were enough checkpoints available for accuracy assessment. Table 6 and figure 10 show the number and identification of GCPs used to process the MS and RGB imagery. In particular, these GCPs were used to evaluate the potential influence of the number of GCPs used during postprocessing on the

horizontal accuracy of imagery collected during MS flight F2 (August 8) and RGB flight F4 (August 9).

Table 6. List of GCPs used to postprocess UAS imagery at GCB.

| MS Flight F2 GCPs | | | RGB Flight F4 GCPs | | |
|---|---|---|---|---|---|
| 10 Ct | 8 Ct | 6 Ct | 10 Ct | 8 Ct | 6 Ct |
| BL2_01 | BL2_01 | BL2_01 | BL3_01 | BL3_01 | BL3_01 |
| BL2_03 | BL2_03 | BL2_03 | BL3_04 | BL3_04 | BL3_04 |
| BL2_04 | BL2_04 | BL2_04 | BL3_11 | BL3_11 | BL3_11 |
| BL2_08 | BL2_08 | BL2_08 | BL_019 | BL_019 | BL_019 |
| BL2_11 | BL2_11 | BL2_11 | BL_003 | BL_003 | BL_003 |
| BL_003 | BL_003 | BL_003 | BL_031 | BL_031 | BL_031 |
| BL_014 | BL_014 | | BL3_03 | BL3_03 | |
| BL_019 | BL_019 | | BL3_08 | BL3_08 | |
| BL_028 | | | BL_014 | | |
| BL_031 | | | BL_028 | | |

Figure 10. GCP distribution used during postprocessing at GCB.

## 2.5 Accuracy assessment methods

Horizontal accuracy was calculated using the root mean square error (RMSE) statistic within the horizontal plane. RMSE (equation 1) determines how much error exists between two data sets.

$$RMSE = \sqrt{\frac{1}{N}\sum_{i=1}^{N}\left(x_i - \hat{x}_2\right)^2} \quad (1)$$

where

$(x_i - \hat{x}_2)^2$ = coordinate differences, squared
$N$ = number of checkpoints.

The coincident locations in the imagery and the GCPs not used in postprocessing and reserved for accuracy assessment (herein referred to as *checkpoints* to distinguish them from postprocessing GCPs) were compared to calculate horizontal accuracy using the RMSE and National Standard for Spatial Data Accuracy (NSSDA) (Federal Geographic Data Committee 1998). To determine the coordinates of each checkpoint, the image was displayed in ESRI ArcGIS version 10.6.1 software. The checkpoints were then digitized from the image, and the coordinates were recorded for each location. As described in the USACE Photogrammetric and Lidar Mapping Engineering Manual (EM) (USACE 2015), 20 or more checkpoints for this project size are required to conduct statistically significant accuracy evaluations. In addition, 20 points make a computation at the 95% confidence level possible (Federal Geographic Data Committee 1998). In this study, 25 checkpoints were used in the accuracy assessment. The NSSDA horizontal accuracy is calculated by summing the squared differences between image coordinates and checkpoint coordinates, taking the average of those points, and then taking the square root of the average RMSE. The NSSDA statistic is then determined by multiplying the composite RMSE$x$ and RMSE$y$ value, RMSE$r$, by a value of 1.7308, which represents the standard error of the mean at the 95% confidence level (equation 2). This means that a user of this data set can be confident that the horizontal position of a feature will be within the NSSDA distance 95% of the time.

$$\text{NSSDA (Horizontal Accuracy at 95\% Confidence)} = \text{RMSE}r \times 1.7308 \quad (2)$$

# 3 Results

## 3.1 Field scenario results

Accuracy of the nine flights was evaluated with variations in field scenarios, software processing precision levels, and number of GCPs applied during postprocessing (table 7). The table reports RMSE, NSSDA, and RMSE difference, comparing the differences in accuracy to the data set with the lowest RMSE or best accuracy, while figure 11 shows a graph of the RMSE values by date and flight. On August 7, the UAS base receiver positional accuracy was being transmitted to the GPS on the aircraft without the National Spatial Reference System NSRS coordinate corrections obtained from the OPUS. The RMSE of flight F2 collected on August 7 without using the OPUS corrections was 1.1261 m. Images collected the following two days used an UAS base receiver operating with OPUS corrections and optimal (default) software processing with RMSEs ranging from 0.0467 to 0.9947 m. More specifically, for the MS imagery collected on August 8, the RMSE ranges from 0.0467 m (Flight F6) to 0.0645 m (Flight F7) with an average RMSE difference of 0.0104 m. For the RGB imagery collected on August 9, the RMSE ranges from 0.0589 m (Flight F3) to 0.9947 m (Flight F6), with an average RMSE difference of 0.4608 m. The RGB imagery collected with two different viewing angles (NADIR vs 10° off-NADIR) were also evaluated. Two images collected on August 9 (Flights F2 and F6) were collected at 10° off-NADIR. The RMSE results in table 7 and figure 11 show that flying 10°off-NADIR reduces the accuracy of the images by up to nearly one meter, while the average RMSE difference for flights flown at NADIR is 0.0021 m. RMSE differences between images flown at 120 and 60 m AGL and NADIR vs 10°off-NADIR (RGB Flights F2 vs F6 and Flights F3 vs F4) were minimal with differences being 0.0325 and 0.0041 m, respectively. Thus, when viewing angle was constant, flying altitude had a minimal impact on accuracy, especially for NADIR flights, and the data sets flown at 120 m AGL had a slightly smaller RMSE than those flown at 60 m AGL.

Table 7. Horizontal accuracy of UAS imagery collected at GCB with different field scenarios.

| Date | Flight | UAS base receiver RTK corrected | Number of processing GCPs | Viewing angle | Altitude (m) | Software processing precision level | Sensor | RMSE (m) | NSSDA (m) | RMSE difference (m) |
|---|---|---|---|---|---|---|---|---|---|---|
| 8/7/2018 | F2 | No | 6 | NADIR | 60 | Optimal | MS | 1.1261 | 1.9491 | N/A |
| | | | | | | | | | | |
| 8/8/2018 | F2 | Yes | 6 | NADIR | 60 | Optimal | MS | 0.0563 | 0.0975 | 0.0096 |
| 8/8/2018 | F3 | Yes | 6 | NADIR | 60 | Optimal | MS | 0.061 | 0.1056 | 0.0143 |
| 8/8/2018 | F6 | Yes | 6 | NADIR | 60 | Optimal | MS | 0.0467 | 0.0808 | 0 |
| 8/8/2018 | F7 | Yes | 6 | NADIR | 60 | Optimal | MS | 0.0645 | 0.1117 | 0.0178 |
| | | | | | | | | | | |
| 8/9/2018 | F2 | Yes | 6 | 10° | 120 | Optimal | RGB | 0.9622 | 1.6654 | 0.9033 |
| 8/9/2018 | F3 | Yes | 6 | NADIR | 120 | Optimal | RGB | 0.0589 | 0.1018 | 0 |
| 8/9/2018 | F4 | Yes | 6 | NADIR | 60 | Optimal | RGB | 0.063 | 0.109 | 0.0041 |
| 8/9/2018 | F6 | Yes | 6 | 10° | 60 | Optimal | RGB | 0.9947 | 1.7215 | 0.9358 |

Figure 11. RMSE results for the nine orthomosaic products collected at GCB.

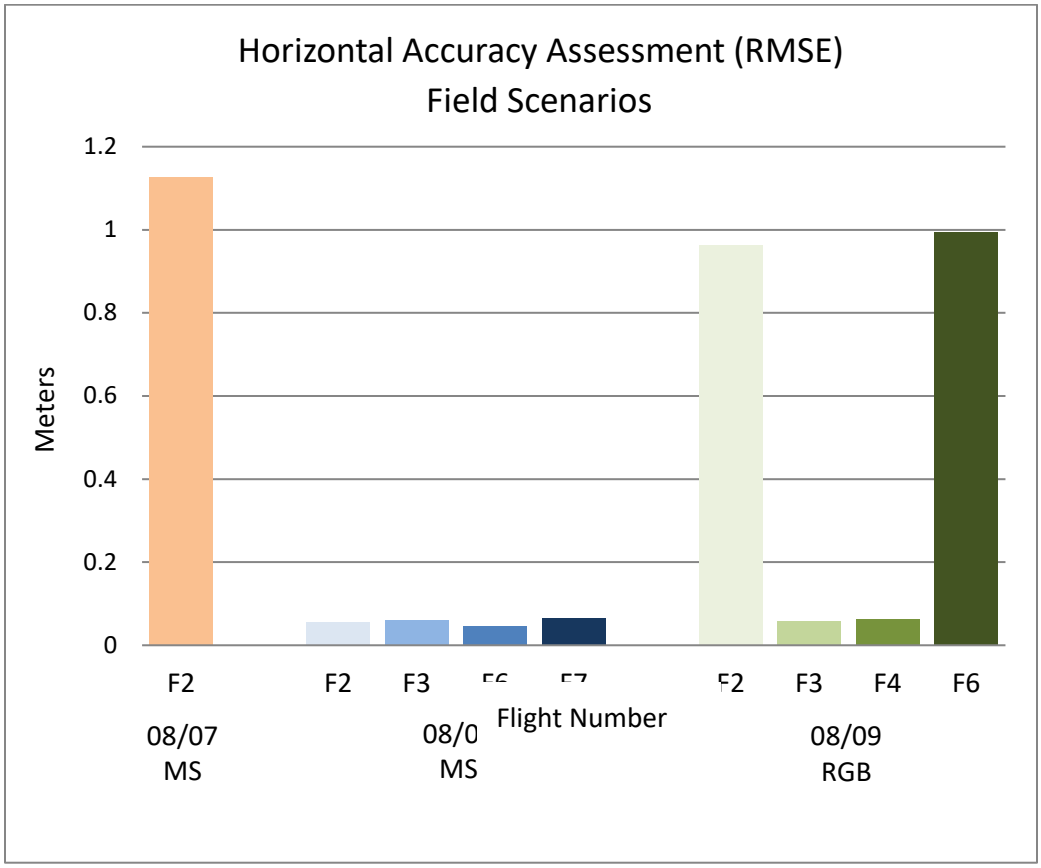

## 3.2 Software processing precision level results

Table 8 and figure 12 show the accuracy of two data sets with various software processing precision levels applied. The RMSEs of the MS imagery (Flight F2) range from 0.0563 to 0.0644 m (ranging from optimal to low processing levels, respectively), with an average RMSE difference of 0.0052 m. In contrast, the RMSEs of the RGB imagery (Flight F4) range from 0.063 to 0.0642 m (ranging from optimal to low processing levels, respectively), with an average RMSE difference of 0.0006 m. Thus, the highest horizontal accuracy is achieved with the optimal (default) processing precision level; however, in this example, the difference in RMSEs between processing levels is minimal, regardless of the sensor type. Furthermore, the average RMSE difference is close to the limit of survey (to within 5 mm for the RTK-GPS equipment used). While care was taken to digitize the center of the checkpoints, some amount of error may be due in part to the digital placement (for example, heads-up digitizing) of the checkpoint locations. In this case, some of the differences in accuracy are so small and close to the limits of the survey that it likely would not impact data application.

Table 8. Horizontal accuracy of UAS imagery collected at GCB with different Pix4DMapper software processing precision levels.

| Date | Flight | Number of processing GCPs | Viewing angle | Altitude (m) | Software processing precision level | Sensor | RMSE (m) | NSSDA (m) | RMSE difference (m) |
|---|---|---|---|---|---|---|---|---|---|
| 8/8/2018 | F2 | 6 | NADIR | 60 | Optimal | MS | 0.0563 | 0.0975 | 0 |
| 8/8/2018 | F2 | 6 | NADIR | 60 | High | MS | 0.0638 | 0.1104 | 0.0075 |
| 8/8/2018 | F2 | 6 | NADIR | 60 | Low | MS | 0.0644 | 0.1114 | 0.0081 |
| | | | | | | | | | |
| 8/9/2018 | F4 | 6 | NADIR | 60 | Optimal | RGB | 0.063 | 0.109 | 0 |
| 8/9/2018 | F4 | 6 | NADIR | 60 | High | RGB | 0.0635 | 0.101 | 0.0005 |
| 8/9/2018 | F4 | 6 | NADIR | 60 | Low | RGB | 0.0642 | 0.111 | 0.0012 |

Figure 12. RMSE results for Flights F2 and F4 with different Pix4DMapper software processing precision levels.

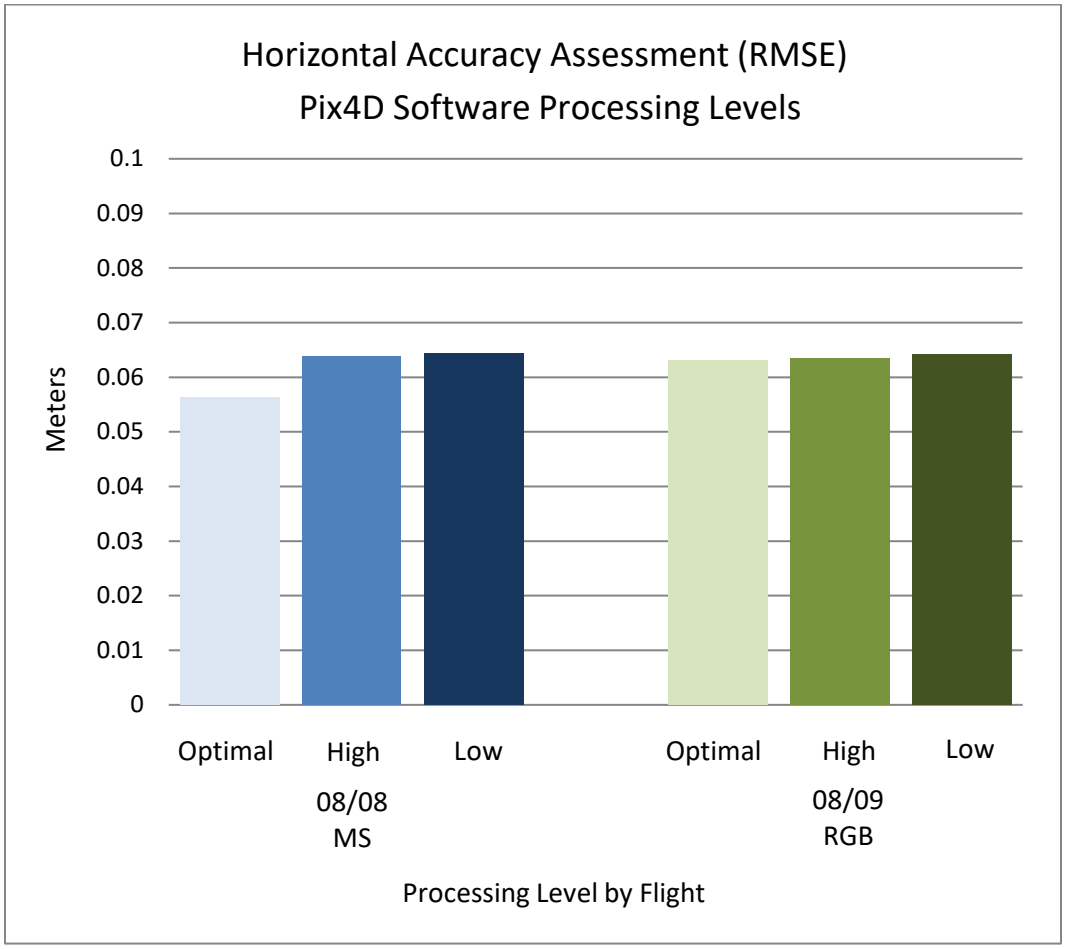


### 3.2.1 Software processing time results

For the results presented in table 8 and figure 12, it is likewise important to weigh the trade-offs between processing time with respect to the various processing precision levels and potential gains or losses in accuracy. This trade-off can be important, because processing data sets at the high level takes additional time compared to processing at the optimal (default) or low levels, and depending on the application of the data, the gains or losses in horizontal accuracy may or may not be important. Table 9 reports processing times at various processing precision levels (optimal, high, and low) for the generation of reflectance mosaics, orthomosaics and point clouds for the same two flight examples, MS flight F2 (August 8) and RGB flight F4 (August 9). In general, the product generation time is longest with the high software processing level and shortest with the low software processing level. While the product generation time for the optimal (default) software processing level falls between the high and low levels, it

is generally closer in time to the low level. For the MS example, the optimally processed reflectance mosaic is produced approximately seven minutes faster than the highly processed version, with a gain of 0.0075 m in horizontal accuracy. Furthermore, the MS postprocessing requires five reflectance images (one per band) to create a single five-band composite image, resulting in a 35-minute time savings. In the RGB example, the optimally processed version has only a very slight gain of 0.0005 m in accuracy, yet the time savings is well over an hour compared to the highly processed version. And even though point clouds were not evaluated in this study, they are routinely generated products, and in this example, the trend shows that it takes anywhere from 3.5 to 21 times the amount of time to develop the highest-density point clouds over the optimal and low levels, respectively. The reduction in time to produce image products at the optimal (default) level, while still optimizing accuracy, is a noted benefit. That in turn can result in significant time savings with larger project areas or when many images are required.

Table 9. Examples of Pix4DMapper software processing times to generate data products at various processing precision levels for GCB. Time units are as follows: h=hours; m=minutes; s=seconds.

| Date | Flight | Sensor | Number of processing GCPs | Software processing precision level | Reflectance generation time | Orthomosaic generation time | Point cloud generation time | Average density (per m³) |
|---|---|---|---|---|---|---|---|---|
| 8/8/2018 | F2 | MS | 6 | High | 29m:03s | 24m:14s | 5m:44s | 233.08 |
| 8/8/2018 | F2 | MS | 6 | Low | 20m:27s | 12m:57s | 1m:01s | 18.4 |
| 8/8/2018 | F2 | MS | 6 | Optimal | 22m:21s | 13m:31s | 1m:52s | 64.22 |
| 8/9/2018 | F4 | RGB | 6 | High | N/A | 2h:21m:23s | 2h:09m:42s | 20,594.0 |
| 8/9/2018 | F4 | RGB | 6 | Low | N/A | 41m:12s | 6m:50s | 2,049.26 |
| 8/9/2018 | F4 | RGB | 6 | Optimal | N/A | 59m:17s | 36m:35s | 6,528.37 |

## 3.3 Number of GCPs applied during postprocessing results

Table 10 and figure 13 show the horizontal accuracy of two data sets with different numbers of GCPs applied during postprocessing (0, 6, 8, or 10). The RMSEs of the MS imagery (Flight F2) range from 0.4535 to 0.0627 m (ranging from 0 to 10 GCPs), with an average RMSE difference of 0.1001 m for all four data sets (including the image processed without GCPs) or an average RMSE difference of 0.0022 m for three data sets (excluding the image processed without GCPs). For the RGB imagery (Flight F4), the

RMSEs range from 0.3221 to 0.0691 m (ranging from 0 to 10 GCPs), with an average RMSE difference of 0.0683 m for all four data sets (including the image processed without GCPs) or an average RMSE difference of 0.0047 m (excluding the image processed without GCPs). Thus, when the data sets are processed without GCPs, the horizontal accuracy decreases by an average of 0.3283 m between the two sensor types, which is considerable compared to RMSE differences in data sets processed with six or more GCPs. Typically, onboard RTK-GPS is expected to improve horizontal accuracy, but in this case, the GPS signal interruptions encountered during the flights may have been a limiting factor.

Regardless of onboard RTK-GPS corrections on the platform, in this example, having a minimal number of well distributed GCPs increases accuracy by a factor of five or more (depending on the sensor) and is particularly helpful for corridor mapping areas. For the RGB, the highest horizontal accuracy achieved is with the data set processed with the software-recommended number of six GCPs (0.063 m), while for the MS, the highest accuracy achieved is with the data set processed with eight GCPs (0.0562 m); however, the MS image processed with the software-recommended six GCPs has a similar RMSE of 0.0563 m. Thus, in this example, regardless of sensor type, including additional GCPs in the postprocessing did not result in substantial horizontal accuracy gains. Yet, the average RMSE differences in MS and RGB data sets processed with 6, 8, and 10 GCPs were relatively small regardless of sensor type (0.0022 to 0.0047 m, respectively). As with the different software processing levels, some amount of error may be due in part to the heads-up digitizing of the checkpoint locations, and differences are close to the limits of survey. In summary, for this study, using an optimal (software-recommended) number of GCPs resulted in considerable horizontal accuracy gains as compared to data processed without GCPs; however, including additional GCPs over the recommended number did not result in substantial horizontal accuracy gains. Again, this relationship can be important when weighing trade-offs related to schedules and budgets, because collecting more GCPs can be time consuming in the field.

Table 10. Horizontal accuracy of UAS imagery collected at GCB with different numbers of GCPs applied during postprocessing.

| Date | Flight | Number of processing GCPs | Viewing angle | Altitude (m) | Software processing precision level | Sensor | RMSE (m) | NSSDA (m) | RMSE difference (m) |
|---|---|---|---|---|---|---|---|---|---|
| 8/8/2018 | F2 | 0 | NADIR | 60 | Optimal | MS | 0.4535 | 0.7848 | 0.3973 |
| 8/8/2018 | F2 | 6 | NADIR | 60 | Optimal | MS | 0.0563 | 0.0975 | 0.0001 |
| 8/8/2018 | F2 | 8 | NADIR | 60 | Optimal | MS | 0.0562 | 0.0973 | 0 |
| 8/8/2018 | F2 | 10 | NADIR | 60 | Optimal | MS | 0.0627 | 0.1086 | 0.0065 |
| | | | | | | | | | |
| 8/9/2018 | F4 | 0 | NADIR | 60 | Optimal | RGB | 0.3221 | 0.5576 | 0.2591 |
| 8/9/2018 | F4 | 6 | NADIR | 60 | Optimal | RGB | 0.063 | 0.109 | 0 |
| 8/9/2018 | F4 | 8 | NADIR | 60 | Optimal | RGB | 0.071 | 0.1223 | 0.008 |
| 8/9/2018 | F4 | 10 | NADIR | 60 | Optimal | RGB | 0.0691 | 0.111 | 0.0061 |

Figure 13. RMSE results for Flights F2 and F4 with different numbers of GCPs applied during postprocessing.

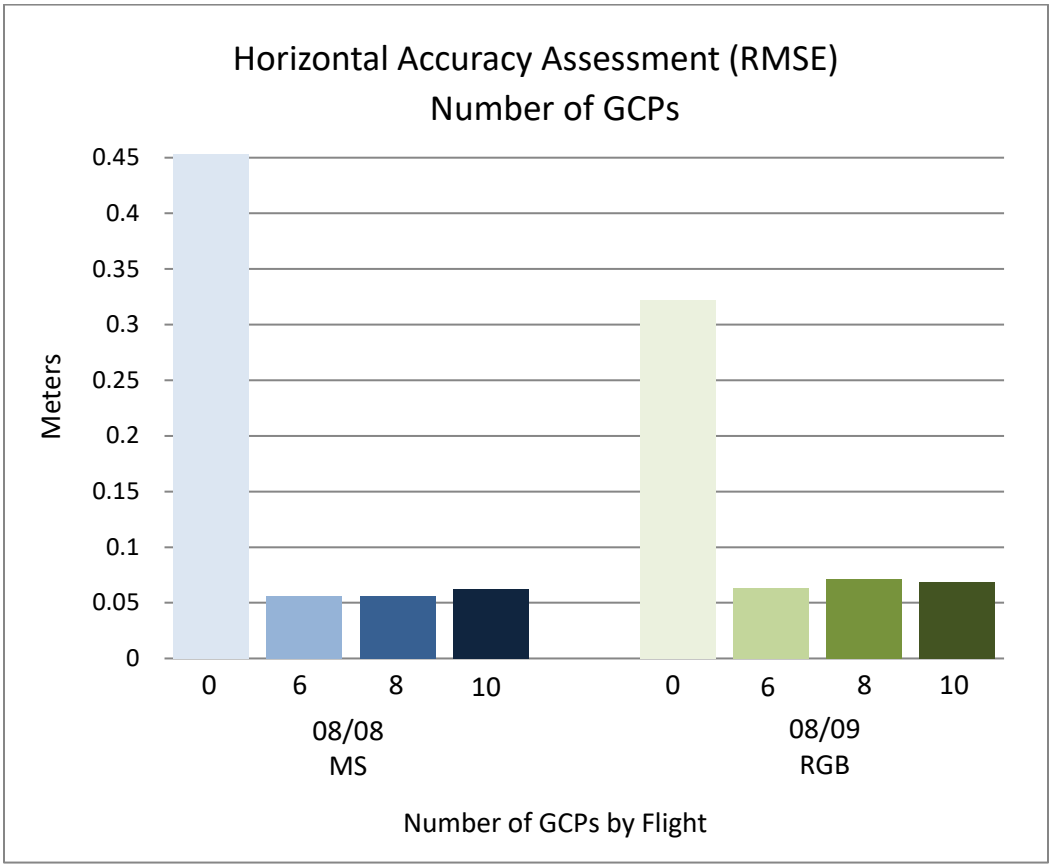

## 3.4 USACE accuracy standards assessment

The accuracy results were further compared to accuracy standards designated by the USACE EM (USACE 2015), which are in part based on guidelines set forth by the American Society of Photogrammetry and Remote Sensing (ASPRS) (ASPRS 2015). As such, the EM provides general guidelines for determining image accuracy at three distinct class levels according to pixel size. The guidelines further state that Highest accuracy represents the highest level for a specified resolution given technologies available at the time the EM was published. Values specific to the Highest accuracy are meant to meet applications in cases where horizontal accuracies are of critical importance and are able to be achieved by sufficient sensor technology, ground control, and other parameters. Values specific to the Standard high accuracy are meant to address needs for standard level of high quality and high accuracy geospatial mapping applications (for example, ASPRS Class 1) and meets the large majority of USACE project standards. Conversely, Lower accuracy is considered appropriate for visualization purposes when higher accuracies are not required. Data sets processed for this study show RMSE values color-coded in tables 11–13, using the color key provided and listing the same data sets by field scenario and processing parameters as shown in tables 7–10.

The MS imagery falls primarily into the Standard high accuracy class, with the exception of the August 7 flight that was collected without using the OPUS corrections. And while none met the Highest accuracy data standard, Flight F6 came close to the mark. In contrast, the RGB imagery falls outside the Lower class accuracy standard. This is not surprising for the data collected at 10°off-NADIR since it can be seen to greatly reduce horizontal accuracy in this study. However, both RGB data sets collected at NADIR, while closer to the lower class accuracy cutoff, still fall outside the mark. This is likely due to a couple of reasons.

The first reason is that the USACE EM accuracy guidelines were developed for large- and medium-format cameras. Thus, the guidelines did not include examples for cameras capable of such high spatial resolutions, and despite providing a flexible solution based on pixel size, which can be translated to very high spatial resolution data, the guidelines may warrant revision that are specific to UAS cameras. If the imagery were resampled to a coarser spatial resolution, it could result in meeting higher class

accuracy standards, but the objective of this study was to evaluate UAS data products at their full spatial resolution potential.

The second reason has to do with potential limits of survey (to within 5 mm for the RTK-GPS equipment used to mark the locations of GCPs). When the GCPs were digitized to identify checkpoint locations in the imagery, they were displayed at the highest scale possible to make sure that the center of the lid was digitized. Even with the care taken to digitize the center of the checkpoints, the head-ups digitizing of the targets may be responsible for at least part of the error and why the RGB imagery (with such high spatial resolutions) does not meet higher accuracy standards. Future collection and accuracy assessment of data with such high spatial resolutions may require revised methods, such as using a PK or other survey nail to mark the exact middle of the target and better ensuring that the point surveyed in the field is as close to the same location chosen for comparison from the imagery. With such high spatial resolution, there could be at least 2 pixels of error associated with digitizing the center of the checkpoint and a reason why the assessment shows that the data fall just outside the lower class accuracy.

1. Highest accuracy: $RMSE_x$ and $RMSE_y \leq 1$ pixel, blue
2. Standard high accuracy: $RMSE_x$ and $RMSE_y$ 2 pixels, green
3. Lower accuracy: $RMSE_x$ and $RMSE_y \geq 3$ pixels, orange

Table 11. Class accuracy of UAS imagery collected at GCB with different field scenarios.

| Date | Flight | Ground sampling distance (cm) | 1 pixel size (cm) | 2 pixel size (cm) | 3 pixel size (cm) | RMSE (cm) |
|---|---|---|---|---|---|---|
| 8/7/2018 | F2 | 3.53 | 3.53 | 7.06 | 10.59 | 112.61: orange |
| | | | | | | |
| 8/8/2018 | F2 | 3.64 | 3.64 | 7.28 | 10.92 | 5.63: green |
| 8/8/2018 | F3 | 3.63 | 3.63 | 7.26 | 10.89 | 6.10: green |
| 8/8/2018 | F6 | 3.57 | 3.57 | 7.14 | 10.71 | 4.67: green |
| 8/8/2018 | F7 | 3.63 | 3.63 | 7.26 | 10.89 | 6.45: green |
| | | | | | | |
| 8/9/2018 | F2 | 1.48 | 1.48 | 2.96 | 4.44 | 96.22: orange |
| 8/9/2018 | F3 | 1.45 | 1.45 | 2.9 | 4.35 | 5.89: orange |
| 8/9/2018 | F4 | 0.69 | 0.69 | 1.38 | 2.07 | 6.3: orange |
| 8/9/2018 | F6 | 0.72 | 0.72 | 1.44 | 2.16 | 99.47: orange |

Table 12. Class accuracy of UAS imagery collected at GCB with different Pix4DMapper software processing precision levels.

| Date | Flight | Number of Processing GCPs | Software processing precision level | Ground sampling distance (cm) | 1 pixel size (cm) | 2 pixel size (cm) | 3 pixel size (cm) | RMSE (cm) |
|---|---|---|---|---|---|---|---|---|
| 8/8/2018 | F2 | 6 | Optimal | 3.64 | 3.64 | 7.28 | 10.92 | 5.63: green |
| 8/8/2018 | F2 | 6 | High | 3.64 | 3.64 | 7.28 | 10.92 | 6.38: green |
| 8/8/2018 | F2 | 6 | Low | 3.64 | 3.64 | 7.28 | 10.92 | 6.44: green |
| | | | | | | | | |
| 8/9/2018 | F4 | 6 | Optimal | 0.69 | 0.69 | 1.38 | 2.07 | 6.3: orange |
| 8/9/2018 | F4 | 6 | High | 0.69 | 0.69 | 1.38 | 2.07 | 6.35: orange |
| 8/9/2018 | F4 | 6 | Low | 0.69 | 0.69 | 1.38 | 2.07 | 6.42: orange |

Table 13. Class accuracy of UAS imagery collected at GCB with different numbers of GCPs applied during postprocessing.

| Date | Flight | Number of processing GCPs | Software processing precision level | Ground sampling distance (cm) | 1 pixel size (cm) | 2 pixel size (cm) | 3 pixel size (cm) | RMSE (cm) |
|---|---|---|---|---|---|---|---|---|
| 8/8/2018 | F2 | 0 | Optimal | 3.64 | 3.64 | 7.28 | 10.92 | 45.35: orange |
| 8/8/2018 | F2 | 6 | Optimal | 3.64 | 3.64 | 7.28 | 10.92 | 5.63: green |
| 8/8/2018 | F2 | 8 | Optimal | 3.64 | 3.64 | 7.28 | 10.92 | 5.62: green |
| 8/8/2018 | F2 | 10 | Optimal | 3.64 | 3.64 | 7.28 | 10.92 | 6.27: green |
| | | | | | | | | |
| 8/9/2018 | F4 | 0 | Optimal | 0.69 | 0.69 | 1.38 | 2.07 | 32.21: orange |
| 8/9/2018 | F4 | 6 | Optimal | 0.69 | 0.69 | 1.38 | 2.07 | 6.3: orange |
| 8/9/2018 | F4 | 8 | Optimal | 0.69 | 0.69 | 1.38 | 2.07 | 7.1: orange |
| 8/9/2018 | F4 | 10 | Optimal | 0.69 | 0.69 | 1.38 | 2.07 | 6.91: orange |

# 4 Discussion and Summary

The horizontal accuracies presented in this study are commensurate with similar studies, such as presented in the USACE ERDC report comparing horizontal and vertical accuracies of coastal RGB imagery and digital surface models using different types of COTS software processing packages (Fischer et al. 2019). In that study, RGB imagery collected in coastal North Carolina (2015-2016) collected at 100 m AGL with a SenseFly eBee micro-UAS (Sensefly, Geneva, Switzerland) and processed with Pix4DMapper software had horizontal accuracies ranging from 0.062 to 0.097 m using four to eight GCPs. Their 2016 data set processed with eight GCPs had an accuracy of 0.062 m, which was in line with the horizontal accuracies of the RGB imagery collected at NADIR for this study: 0.0589 to 0.063 m (120 and 60 m AGL, respectively). However, their results fell within the USACE Standard high accuracy class, because the data were processed at a spatial resolution of 0.036 m. Additionally, Fischer et al. (2019) evaluated data collection strategies, camera settings, and ground control designs in relation to geospatial accuracies. Similar to the findings presented in that report, this case study shows how field scenarios, software procession precision levels, and number of GCPs applied during postprocessing influence horizontal accuracy of image products collected in a coastal corridor mapping area.

In addition to being in line with other studies evaluating field and software parameters, the data collected for this study also shows that it can be used to support a wide range of USACE Civil Works applications. The specifications listed for Civil Works applications specifically identify horizontal and vertical accuracy requirements in the USACE EM (USACE 2015). With the exception of select applications in the Structural Deformation Monitoring Studies/Surveys topic area (for example, crack, joint, and deflection measurements) and the Archeological or Structure Site Plans and Details topic area, many of the data sets collected at GCB met the minimum horizontal accuracy requirements listed for the USACE applications, a number of which involve some level of site monitoring, and are listed below:

1. ($RMSE_{xy}$: 2.5–30 cm) Site Plan for Design Memoranda, Contract Plans and Specifications, etc. for Input to CADD 2-D/3-D Design Files (Locks, Dams, Flood Control Structures.; Grading/Excavation;

Spillways, Concrete Channels, Upland Disposal Areas; Construction In-place Volume Measurement)

2. ($RMSE_{xy}$: 30–240 cm) River and Harbor Navigation Projects: Site Plans, Design, Operation, or Maintenance of Flood Control Structures, Canals, Channels, etc. for Contract Plans or Reports (Levees and Groins; Canals and Waterway Dredging; Beach Renourishment and Hurricane Protection Projects; Project Condition Reports; Revetment Clearing, Grading, and As-built Protection)
3. ($RMSE_{xy}$: 120 cm–0.10 km) Geotechnical and Hydrographic Site Investigation Surveying Accuracies for Project Construction (Hydrographic Contract Payment and P&S; Hydrographic Project Condition; Hydrographic Reconnaissance; Geotechnical Investigative Core Borings, Probings)
4. ($RMSE_{xy}$: 120 cm) General Planning and Feasibility Studies, Reconnaissance Reports, Permit Applications, etc.
5. ($RMSE_{xy}$: 120–450 cm) GIS Feature Mapping (Area- and Project-Wide Mapping Control Network to Support Overall GIS Development; Soil and Geologic Classification Maps, Well Points; Cultural and Economic Resources, Historic Preservation; Land Utilization GIS Classifications; Regulatory Permit General Locations; Socio-economic GIS classifications; Land Cover Classification)
6. ($RMSE_{xy}$: 0.625 cm) Archeological or Structure Site Plans & Details (Including Non-topographic, Close Range, Photogrammetric Mapping)
7. ($RMSE_{xy}$: 0.2 mm–3 cm) Structural Deformation Monitoring Studies/Surveys (Reinforced Concrete Structures—Locks, Dams, Gates, Intake Structures, Tunnels, Penstocks, Spillways, Bridges, etc.; Earth/Rock Fill Structures; Crack, joint, and deflection measurements)
8. ($RMSE_{xy}$: 240 cm) Flood Control and Multipurpose Project Planning, Floodplain Mapping, Water Quality Analysis, and Flood Control Studies
9. ($RMSE_{xy}$: 240 cm) Federal Emergency Management Agency Flood Insurance Studies

This study examines the influence of field data collection scenarios, software processing precision levels, and the number of GCPs applied during postprocessing to horizontal accuracies. All of these decisions have a direct bearing on the level of product accuracy, and this study shows an example of how to produce products that have potential use in coastal monitoring and other Civil Works applications. More specifically, such monitoring examples can include site plans, beach renourishment and

hurricane protection projects, project conditions, planning and feasibility studies, floodplain mapping, water quality analysis, flood control studies, emergency management, and ecosystem restoration. Many of these examples require field monitoring, in which site access and impacts to resources can be limiting factors, yet detailed site data are required. UAS data, when collected under specific scenarios and processed appropriately, can help bridge the gap between extensive field data collection requirements and geographic coverage at the appropriate project scale. Furthermore, this case study attempts to illustrate collection and processing scenarios in which horizontal accuracies can be maximized while minimizing time and costs associated with software processing and field data collection. Yet, a thorough understanding of how the data will be applied is critical for selecting the appropriate collection and processing parameters, and understanding those trade-offs in relation to accuracy requirements will save time and money.

As onboard GPS solutions continue to advance, the need for GCPs will likely decrease, helping to minimize survey time and costs. In this study, RTK onboard the UAS platform, along with a minimum of six GCPs, increased horizontal accuracies of orthoimages considerably (on the order of 26 to 40 cm) in contrast to orthoimages processed without GCPs. As such, RTK, while considered an advancement in providing real-time corrections to location data, is still subject to challenges such as interruptions in communication with the base station, which can potentially impact location data integrity. Alternatively, newer Post-Processed Kinematic (PPK) correction solutions do not rely on base station correction links and are applied after data collection, offering a more flexible and robust option. It enables less reliance on GCPs; however, including some amount of GCPs ensures integrity and validation to produce the best data possible—especially in coastal corridor mapping configurations.

The data collection and accuracy assessment achieved in this effort highlights procedures resulting in high resolution UAS MS and RGB imagery that can be used to meet a variety of USACE project needs. More specifically, this examination of data collection and processing methods shows that UAS imagery serves to complement the wide variety of remotely sensed data solutions to support flood risk management applications in the coastal zone, where corridor mapping considerations are critical for collecting high integrity data. In this study, high accuracy is

required to best link ground measurements describing dune vegetation characteristics with image values to establish relationships that assist with monitoring. Future data analysis will include comparisons of imagery and ground measurements to determine appropriate UAS image–derived metrics for vegetation characterization. The accuracy assessment in this study helps ensure the most appropriate data to conduct such research, and ultimately, it helps demonstrate how UAS data can be collected and evaluated to meet monitoring and management activities in USACE projects.

# References

Acosta, A., Carranza, M.L., Izzi, C.F. 2005. Combining Land cover mapping for coastal dune with vegetation analysis. *Appl Veg Sci,* 8(2):133–138.

Affleck, D., Gregoire, T. and Valentine, H. 2005. Design unbiased estimation in line intersect sampling using segmented transects. *Environ Ecol Stat*, 12(2): 139-154.

American Society of Photogrammetry and Remote Sensing (ASPRS). 2015. ASPRS positional accuracy standards for digital geospatial data. *Photogrammetric Engineering and Remote Sensing,* 81(3): A1–A26.

Bruder, B.L., Renaud, A.D., Spore, N.J. and Brodie, K.L. 2018. Evaluation of Unmanned Aircraft Systems for Flood Risk Management: Field Experiment Conspectus. ERDC/CHL SR-18-2. Special Reports Collection. Vicksburg, MS: US Army Engineer Research and Development Center.

Chen, B., Yang, Y., Wen, H., Ruan, H., Zhou, Z., Luo, K., and Zhong, F. 2018. High-resolution monitoring of Beach topography and its change using unmanned aerial vehicle imagery. *Ocean Coast Manag*, 160: 103–116.

Choi, S.K., Lee, S.K., Jung, S.H., Choi, J.W., Choi, D.Y., an Chun, S.J. 2016. Estimation of Fractional Vegetation Cover in Sand Dunes Using Multi-spectral Images from Fixed-wing UAV. *Journal of the Korean Society of Surveying, Geodesy, Photogrammetry and Cartography*, 4(4). Korean Society of Surveying, Geodesy, Photogrammetry and Cartography.

Drummond, C.D., Hartley, M.D., Turner, I.L., Matheen, A., Nashwan, A., and Glamore, W.C. 2015. UAV applications to coastal engineering [online]. In: Australasian Coasts & Ports Conference 2015: 22nd Australasian Coastal and Ocean Engineering Conference and the 15th Australasian Port and Harbour Conference. Auckland, New Zealand: Engineers Australia and IPENZ, 267-272.

Fischer, R.L., Ruby, J.G., Armstrong, A.J., Edwards, J.D., Spore, N.J. and Brodie, K.L. 2019. Geospatial Accuracy of Small Unmanned Airborne System Data in the Coastal Environment. ERDC SR-19-1. Special Reports Collection. Vicksburg, MS: US Army Engineer Research and Development Center.

Gonçalves, J.A. and Henriques, R. 2015. UAV photogrammetry for topographic monitoring of coastal areas. *ISPRS J Photogramm Remote Sens*, 104: 101–111.

Green, D.R., Hagon, J.J., and Gomez, C. 2018. Using Low Cost UAVs for Environmental Monitoring, Mapping and Modelling: Examples from the Coastal Zone. In R. R. Krishnamurthy, M. P. Jonathan, S. Srinivasalu, & B. Glaeser (Eds.), *Coastal Management: Global Challenges and Innovations* Elsevier.

Klemas, V. 2001. Remote sensing of landscape-level coastal environmental indicators. *Environmental Management*, 27(1): 47–57.

Klemas, V. 2013. Airborne remote sensing of coastal features and processes: An overview. *J Coastal Res*, 29(2): 239–255.

Klemas, V. 2015. Coastal and Environmental Remote Sensing from Unmanned Aerial Vehicles: An Overview. *J Coastal Res*, 31(5): 1260-1267.

Mancini, F., Dubbini, M., Gattelli, M., Stecchi, F., Fabbri, S., and Gabbianelli, G. 2013. Using unmanned aerial vehicles (UAV) for high-resolution reconstruction of topography: The structure from motion approach on coastal environments, *Remote Sens*ing, 5(12): 6880–6898.

Mumby. P.J., Raines, P.S., Gray, D.A. and Gibson, J.P. 1995. Geographic information systems: A tool for integrated coastal zone management in Belize. *Coastal Management*, 23(2): 111-121.

Nolet, C., Van Puijenbroek, M., Suomalainen, J., Limpens, J., and Riksen, M. 2018. UAV-imaging to model growth response of marram grass to sand burial: Implications for coastal dune development. *Aeolian Res*, 31: 50–61.

Phinn. S.R., Menges, C., Hill, G.J.E. and Stanford, M. 2000. Optimizing remotely sensed solutions for monitoring, modeling, and managing coastal environments. *Remote Sensing of Environment*, 73(2), 117–132.

Scarelli, F.M., Sistilli, F., Fabbri, S., Cantelli, L., Barboza, FOR EXAMPLE, Gabbianelli, G. 2017. Seasonal dune and beach monitoring using photogrammetry from UAV surveys to apply in the ICZM on the Ravenna coast (Emilia-Romagna, Italy). *Remote Sensing Applications: Society and Environment*, 7: 27-39.

Seymour, A.C., Ridge, J.T., Rodriguez, A.B., Newton, E., Dale, J., and Johnston, D.W. 2018. Deploying Fixed Wing Unoccupied Aerial Systems (UAS) for Coastal Morphology Assessment and Management. *J Coastal Res*, 34(3): 704 – 717.

Sturdivant, E.J., Lentz, E.E., Thieler, E.R., Farris, A.S., Weber, K.M., Remsen, D.P., Miner, S., and Henderson, R.E. 2017. UAS-SfM for Coastal Research: Geomorphic Feature Extraction and Land Cover Classification from High-Resolution Elevation and Optical Imagery. *Remote Sens*, 9(1): 1020.

Su, L., and Gibeaut, J. 2017. Using UAS Hyperspatial RGB Imagery for Identifying Beach Zones along the South Texas Coast. *Remote Sens*, *9*: 159.

Suir, G., Reif, M., Hammond, S., Jackson, S., and Brodie, K. 2018. Unmanned Aircraft Systems to Support Environmental Applications within USACE Civil Works. ERDC SR-18-3 Special Reports Collection. Vicksburg, MS: US Army Engineer Research and Development Center.

Thomas, L., Williams, R. and Sandilands, D. 2007. Designing line transect surveys for complex survey regions. *J. Cetacean Res Manage*, 9(1):1–13.

Turner, I.L., Harley, M.D., and Drummond, C.D. 2016. UAVs for coastal surveying. *Coast Eng*, 114: 9–24.

US Army Corps of Engineers (USACE). 2015. *Photogrammetric and LiDAR Mapping*. EM 1110-1-1000. Washington, DC: US Army Corps of Engineers.

US Army Corps of Engineers (USACE). 2017. MYRTLE BEACH REACHES 1 & 3 SAND FENCING AND DUNE VEGETATION SHORE PROTECTION PROJECT. W912HP-17-R-0021. Charleston, South Carolina: US Army Corps of Engineers.

van Puijenbroek, M.E.B., Nolet, C., de Groot, A.V., Suomalainen, J.M., Riksen, M.J.P.M., Berendse, F., and Limpens, J. 2017. Exploring the contributions of vegetation and dune size to early dune development using unmanned aerial vehicle (UAV) imaging. *Biogeosciences*, 14: 5533–5549.

Wozencraft, J., Dunkin, L., Reif, M., and Eisemann, E. 2018. A Spatial Index Approach to Coastal Monitoring: A Florida Case Study. *J Coastal Res*, (81(sp1): 67 – 75.

# REPORT DOCUMENTATION PAGE

*Form Approved*
*OMB No. 0704-0188*



| 1. REPORT DATE *(DD-MM-YYYY)* | 2. REPORT TYPE | 3. DATES COVERED *(From - To)* |
|---|---|---|
| September 2020 | Final | |

**4. TITLE AND SUBTITLE**

Evaluation of Unmanned Aircraft System Coastal Data Collection and Horizontal Accuracy: A Case Study at Garden City Beach, South Carolina

**5a. CONTRACT NUMBER**

**5b. GRANT NUMBER**

**5c. PROGRAM ELEMENT NUMBER**

**6. AUTHOR(S)**

Molly Reif, Scott Bourne, Jennifer Laird, Thomas Berry, Justin Wilkens, Kevin Philley, and Kenneth Matheson

**5d. PROJECT NUMBER**

**5e. TASK NUMBER**

**5f. WORK UNIT NUMBER**

**7. PERFORMING ORGANIZATION NAME(S) AND ADDRESS(ES)**

USACE Engineer Research and Development Center
Environmental Laboratory
3909 Halls Ferry Road
Vicksburg, MS 39180

**8. PERFORMING ORGANIZATION REPORT NUMBER**

ERDC/EL-TR-20-7

**9. SPONSORING / MONITORING AGENCY NAME(S) AND ADDRESS(ES)**

USACE Engineer Research and Development Center
Coastal and Hydraulics Laboratory
3909 Halls Ferry Road
Vicksburg, MS 39180

**10. SPONSOR/MONITOR'S ACRONYM(S)**

**11. SPONSOR/MONITOR'S REPORT NUMBER(S)**

**12. DISTRIBUTION / AVAILABILITY STATEMENT**

Approved for public release; distribution is unlimited.

**13. SUPPLEMENTARY NOTES**

AMSCO 190012, "UAS Support for Coastal Management"

**14. ABSTRACT**

The US Army Corps of Engineers (USACE) aims to evaluate unmanned aircraft system (UAS) technology to support flood risk management applications, examining data collection and processing methods and exploring potential for coastal capabilities. Foundational evaluation of the technology is critical for understanding data application and determining best practices for data collection and processing. This study demonstrated UAS Multispectral (MS) and Red Green Blue (RGB) image efficacy for coastal monitoring using Garden City Beach, South Carolina, as a case study. Relative impacts to horizontal accuracy were evaluated under varying field scenarios (flying altitude, viewing angle, and use of onboard Real-Time Kinematic-Global Positioning System), level of commercial off-the-shelf software processing precision (default optimal versus high or low levels) and processing time, and number of ground control points applied during postprocessing (default number versus additional points). Many data sets met the minimum horizontal accuracy requirements designated by USACE Engineering Manual 2015. Data collection and processing methods highlight procedures resulting in high resolution UAS MS and RGB imagery that meets a variety of USACE project monitoring needs for site plans, beach renourishment and hurricane protection projects, project conditions, planning and feasibility studies, floodplain mapping, water quality analysis, flood control studies, emergency management, and ecosystem restoration.

**15. SUBJECT TERMS**

Coasts; Shorelines; Beaches, Garden City Beach (S.C.); Data collection platforms; Drone aircraft; Remote sensing

| 16. SECURITY CLASSIFICATION OF: | | | 17. LIMITATION OF ABSTRACT | 18. NUMBER OF PAGES | 19a. NAME OF RESPONSIBLE PERSON |
|---|---|---|---|---|---|
| a. REPORT | b. ABSTRACT | c. THIS PAGE | | | Molly Reif |
| Unclassified | Unclassified | Unclassified | SAR | 48 | 19b. TELEPHONE NUMBER *(include area code)* (228) 252-1134 |